Received: 28 March 2023 | Revised: 30 June 2023 | Accepted: 9 August 2023

DOI: 10.4218/etrij.2023-0128

SPECIAL ISSUE

ETRI Journal WILEY

Ultrawideband coupled relative positioning algorithm applicable to flight controller for multidrone collaboration

Jeonggi Yang | **Soojeon Lee**

Mobility Infra Research Section, Electronics and Telecommunications Research Institute, Daejeon, Republic of Korea

Correspondence
Jeonggi Yang, Mobility Infra Research Section, Electronics and Telecommunications Research Institute, Daejeon, Republic of Korea.
Email: jgyang@etri.re.kr

Funding information
ETRI grant, grant/award numbers: 23ZS1200, Fundamental Technology Research for Human-Centric Autonomous Intelligent Systems.

Abstract

In this study, we introduce a loosely coupled relative position estimation method that utilizes a decentralized ultrawideband (UWB), Global Navigation Support System and inertial navigation system for flight controllers (FCs). Key obstacles to multidrone collaboration include relative position errors and the absence of communication devices. To address this, we provide an extended Kalman filter-based algorithm and module that correct distance errors by fusing UWB data acquired through random communications. Via simulations, we confirm the feasibility of the algorithm and verify its distance error correction performance according to the amount of communications. Real-world tests confirm the algorithm's effectiveness on FCs and the potential for multidrone collaboration in real environments. This method can be used to correct relative multidrone positions during collaborative transportation and simultaneous localization and mapping applications.

KEYWORDS
drone, navigation, ultrawideband, vehicular networks

1 | INTRODUCTION

Multidrone collaboration technology is gaining attention as a potential solution to single unmanned aerial vehicle (UAV) operation limitations, such as low battery and restricted payload capacities [1, 2]. Additionally, surveillance and simultaneous localization and mapping (SLAM) performance augmentation technologies are being leveraged to compensate for shortened mission times [3, 4]. A flying ad hoc network was proposed to overcome the drawbacks of communication congestion, poor information exchange between drones, and difficulties in overcoming shadow areas [5, 6]. However, there are several obstacles to resolving these issues algorithmically, such as the absence of an interdrone communication system and a relative positioning system. Commercial cellular long-term evolution, Wi-Fi, and Bluetooth low-energy [7–9] communications systems have been examined; however, their system topologies have changed rapidly and are unsuitable for wide-area drone operation environments. Furthermore, when relying solely on Global Navigation Support System (GNSS) and inertial navigation system (INS) technologies, it is difficult to achieve precise relative position corrections within the GNSS error range. For example, accumulated altitude errors are often significant, and they create havoc for short-distance collaborations. Although motion capture and other precision positioning systems have been effective in laboratory environments, they are often unreliable in real-world applications. Similarly, although the real-time kinematic (RTK) GNSS capability is a practical alternative for many drone missions, it has the

disadvantages of high installation and maintenance costs. To overcome these and other issues, various attempts have been made to develop viable communication and relative position correction techniques.

Interest in ultrawideband (UWB) technologies for drone communication and relative position correction is growing. UWB is a short-distance radio specification that offers the advantages of low interference with existing communication systems and excellent distance measurement precision. Recently, UWB has been standardized for use in object location tracking, such as for air tags, smartphones, and vehicle keys [10]. Various studies and products utilizing UWB positioning systems for indoor robots have been developed [11, 12]. UWB is also suitable for multidrone collaboration environments as it allows additional side-channel information exchanges. Moreover, UWB's precise distance measurement capability enables good positioning in locations where GNSS/INS may not function, making it an excellent alternative.

Studies on UWB-based relative position calibration and precise flight formations are actively under way. As such, the navigation methods are in focus, pertaining to calculating the positions of multiple drones and UWB anchors in GNSS-denied environments [13]. For example, a relative localization algorithm for distance-based formation control was proposed that combines drone odometry and UWB data [14]. Assuming that the drones fly at the same altitude, the algorithm successfully forms a two-dimensional spatial shape. An onboard UWB and visual-inertial odometry fusion technique can also be used to precisely estimate relative positions [15], even in environments with no directional coordinate system. Thus, the relative positions of drones can be orchestrated in a decentralized manner via the exchange of odometric information. Although many studies have focused on scenarios without GNSS, there has been growing interest in UWB solutions. This is also true for the GPS-enabled environments. Some studies have used combinations of UWB, GNSS, and INS as anchor tag systems to obtain ground-truth coordinates, rather than for relative localization among multiple robots [16, 17].

In this study, we propose a decentralized UWB/GNSS/INS fusion algorithm that enables universal collaboration between short-range drones. In contrast to other studies that assume a GNSS-free environment, our objective is to obtain accurate formations without the need for RTK-GNSS by actively utilizing UWB, GNSS, and INS information together. Specifically, the proposed algorithm shares position information and distance measurements using random access UWB to correct existing GNSS/INS extended Kalman filter (EKF)-derived navigation values (Figure 1). The proposed algorithm exhibits two beneficial characteristics. First, it requires fewer calculations than other systems, and communication efficiency is optimized by actively utilizing the navigation information of the GNSS/INS. Second, the algorithm assumes a random gossip environment in which data are acquired and filtered from all neighbors. Considering the general unreliability of UWB communications induced by a short communication range and obstruction by objects, our algorithm is capable of operating in an asynchronous random access environment.

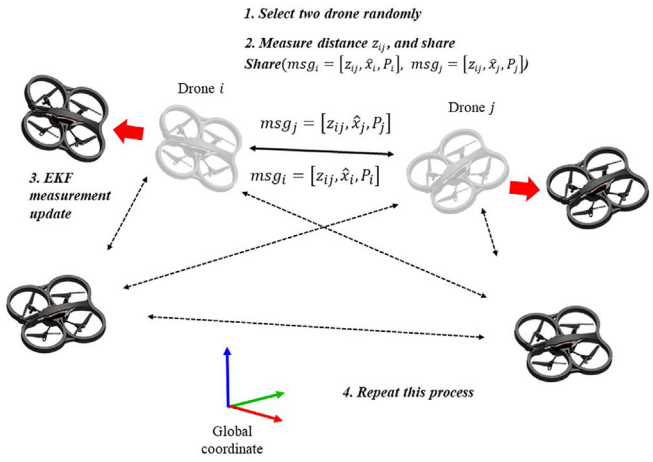

FIGURE 1 Ultrawideband-coupled relative positioning algorithm.

2 | UWB-BASED RELATIVE POSITIONING ALGORITHM

2.1 | Problem statement

The notations used in this study are listed in Table 1. We consider a situation in which n drones maintain close proximity for collaboration, forming a UWB peer-to-peer communication network. In a three-dimensional (3D) space, n drones use the same global coordinate system, wherein each drone estimates its position using a GNSS/INS-based EKF; thus, each drone maintains its own position and covariance matrix. We assume that the drones are capable of simultaneously measuring and sharing distances, estimated positions, and covariance matrices over UWB. The UWB distance measurement is represented as the addition of Gaussian noise th the actual distance, with a predefined standard deviation of 0.1 m, as depicted in (1). The network is assumed to be nondirectional and fully connected.

TABLE 1 Notations used in problem statements.

Notations	
N	The set of drones, where $N = \{1, 2, 3, ..., n\}$
E	The set of edges, where $E = \{(i,j) \mid \text{linked } i, j \in N\}$
x_i	Drone i's 3D position vector: $x_i(t) = [pos_x, pos_y, pos_z]^T$
$\hat{x}_i$	Drone i's estimated position vector
P_i	Drone i's position covariance matrix
x	All drones' position vectors: $x = [x_1^T, x_2^T, ..., x_n^T]^T$
$\hat{x}$	All drone's estimated position vectors
P	All drones' position covariance matrices: $P = \text{diag}(P_1, P_2, ..., P_n)$
$\hat{x}_{ij}$	Augmented estimated position vector: $\hat{x}_{ij} = [\hat{x}_i^T, \hat{x}_j^T]^T$
P_{ij}	Augmented covariance matrix: $P_{ij} = \text{diag}(P_i, P_j)$
z_{ij}	UWB distance measurement between Drones i and j.
p_{ij}	Drone i's probability of communicating with Drone j per iteration
msg_i	Drone i's message shared when communication occurs
$*(k)$	The state at iteration k; the $*$ can be replaced with any value or vector
$*[n:m]$	The sliced vector, $(*[n:m])_a = (*)_{n \le a < m}$; the $*$ can be replaced with any vector

Algorithm 1: EKF-based Relative Positioning

1 Update global position by GNSS/INS position estimator

$$\hat{x}_i(k),\ P_i(k) \tag{2}$$

2 Try random communication with neighborhood

$$msg_i(k) = [z_{ij}(k), \hat{x}_i(k), P_i(k)],\quad msg_j(k) = [z_{ij}(k), \hat{x}_j(k), P_j(k)] \tag{3}$$

3 **If** receive other drone's msg **then**

4 Make augmented state and covariance matrix

$$\hat{x}_{ij}(k) = [\hat{x}_i(k)^T, \hat{x}_j(k)^T]^T,\quad P_{ij}(k) = \begin{bmatrix} P_i(k) & \mathbf{0} \\ \mathbf{0} & P_j(k) \end{bmatrix} \tag{4}$$

5 Set Jacobian matrix as H

$$dir_{ij}(k) = \frac{(\hat{x}_i(k) - \hat{x}_j(k))}{\|\hat{x}_i(k) - \hat{x}_j(k)\|} \tag{5}$$

$$H_{ij} = [dir_{ij}(k)^T \quad -dir_{ij}(k)^T] \tag{6}$$

6 UWB distance-based EKF measurement update

$$S = (H_{ij} P_{ij}(k) H_{ij}^T + R) \tag{7}$$

$$K = P_{ij}(k) H_{ij}^T S^{-1} \tag{8}$$

$$\hat{x}_{ij}(k+1) = \hat{x}_{ij}(k) + K(z_{ij}(k) - H_{ij}\hat{x}_{ij}(k)) \tag{9}$$

$$P_{ij}(k+1) = (I - K_{ij} H_{ij}) P_{ij}(k) \tag{10}$$

7 Extract own state from augmented state

$$\hat{x}_i(k+1) = \hat{x}_{ij}(k+1)[0{:}3],\quad P_{ij}(k+1) = P_{ij}(k+1)[0{:}3][0{:}3] \tag{11}$$

end

8 Go to 1

$$z_{ij}(k) = \|x_i(k) - x_j(k)\| + \eta,\ \ \eta \sim N(0, \sigma^2)\ \ (\sigma = 0.1). \tag{1}$$

The goal of the proposed algorithm is to correct position estimates to minimize the sum of the magnitudes of the differences between true and estimated distances. As such, the algorithm must have a low computational complexity and be implemented as a flight controller (FC) that operates in unreliable UWB environments caused by short distances and obstacles. The drone must be capable of adjusting its navigation performance and communication load so that UWB communications can be used for navigation corrections and general data communications.

2.2 | EKF-based relative positioning algorithm

The proposed algorithm performs random EKF measurement updates based on UWB-based GNSS/INS communication information. The pseudocode is presented in Algorithm 1.

The proposed algorithm is constructed as depicted in (2) and is based on the estimated position and its covariance obtained through GNSS/INS integration. Next, each drone attempts random UWB communications, which refers to the process of measuring the distance between two drones and sharing the estimated positions and covariances with others. This operation is expressed as (3). Drone i has a probability of communicating with Drone j during each iteration, and because the network is assumed to be fully connected, the probability is assumed to be the same for all drones. After the communication attempt, the drones that have exchanged messages proceed with the steps defined in (4)–(11), whereas the drone without any exchanged messages does not update anything and returns to the GNSS/INS update step. When messages are exchanged, a drone augments its state and covariance with the received message information to form a six-dimensional (6D) augmented estimated position vector, as expressed in (4). Covariance matrix P_{ij} is augmented to match the covariance of the corresponding drone in each diagonal term, and the cross-correlation is assumed to be a **0**-matrix. A standard EKF measurement algorithm is employed that

utilizes distance information z_{ij} for measurements. The measurement matrix, shown in (6), is obtained by computing the Jacobian matrix with (1). When computing the innovation covariance using (7), parameter R represents the measurement error, which is typically set as the UWB measurement error; however, it can be fine-tuned by the user. The Kalman gain is calculated using (8), and the augmented state vector and covariance are updated according to (9) and (10), respectively. Because the desired information lies within the first three states of the augmented vector, it is extracted using (11) and is input as the state and error covariance for the next iteration.

This algorithm reduces computational complexity by decreasing the number of Kalman filter states through random sampling techniques. Referring to a previous study that proposed an algorithm for multiple drones and UWB anchors to perform self-localization using an EKF in a GPS-denied environment, the positions of the moving agents are included as states of the Kalman filter. The computational complexity of the EKF increases exponentially with the cube of the state dimension. Hence, if we consider an algorithm for k drones, its computational complexity can be expressed as $O(k^3)$. Instead of acquiring and updating information for all edges, we adopt a strategy of updating only the randomly acquired edge information. Therefore, the computational complexity of updating a single edge remains constant. If we calculate the algorithm for a single drone by considering all neighboring drones, the computational complexity is $O(k)$. In a scenario in which all edges in the network communicate, the computational complexity becomes $O(k^2)$. In terms of computational complexity, the efficiency of the proposed algorithm increases as the number of neighbors connected through the network increases.

2.3 | Simplified algorithm for FC

Because drone FCs are typically based on advanced reduced-instruction set Cortex M microcontrollers, the algorithm must be optimized to minimize the number of computations required. As such, although it is based on a six-dimensional (6D) Kalman filter, only the 3D state can be used. When (9) and (11) are expressed in block matrix forms, they become equivalent to (13) and (14). Algorithm 2 is designed to process only the updated information for $x_i(k)$ and $P_i(k)$ in (11) and (12). By eliminating the computation information for $x_j(k)$ and $P_j(k)$, the original 6D states are reduced to 3D states by eliminating the computational information for $\hat{x}_j(k)$ and $P_j(k)$.

$$\begin{bmatrix}\hat{x}_i(k+1)\\ \hat{x}_j(k+1)\end{bmatrix} = \begin{bmatrix}\hat{x}_i(k)\\ \hat{x}_j(k)\end{bmatrix} + \frac{1}{S}\begin{bmatrix}P_i(k)dir_{ij}(k)\\ -P_j(k)dir_{ij}(k)\end{bmatrix} * \left(z_{ij}(k) - \left\|\hat{x}_i(k) - \hat{x}_j(k)\right\|\right), \quad (13)$$

$$\begin{bmatrix}P_i(k+1) & P_{ij}(k+1)_{12}\\ P_{ij}(k+1)_{21} & P_j(k+1)\end{bmatrix} = \begin{bmatrix}A_{11} & A_{12}\\ A_{21} & A_{22}\end{bmatrix}\begin{bmatrix}P_i(k) & \mathbf{0}\\ \mathbf{0} & P_j(k)\end{bmatrix},$$
$$A_{11} = I - \frac{1}{S}P_i(k)dir_{ij}(k)dir_{ij}(k)^{\mathrm{T}}. \quad (14)$$

Algorithm 2: Simplified Flight Control Algorithm

1. Update global position by GNSS/INS position estimator
   $$\hat{x}_i(k),\ P_i(k)$$
2. Try random communication with neighborhood
   $$msg_i(k) = [z_{ij}(k), \hat{x}_i(k), P_i(k)],$$
   $$msg_j(k) = [z_{ij}(k), \hat{x}_j(k), P_j(k)]$$
3. **If** receive other drone's msg **then**
4. Calculate Kalman gain and innovation
   $$dir_{ij}(k) = \frac{(\hat{x}_i(k) - \hat{x}_j(k))}{\|\hat{x}_i(k) - \hat{x}_j(k)\|}$$
   $$S = dir_{ij}(k)^T * (P_i + P_j) * dir_{ij}(k) + R \quad (15)$$
   $$K = \frac{1}{S}P_i(k)dir_{ij}, \quad (16)$$
   $$innov = \left(z_{ij}(k) - \|\hat{x}_i(k) - \hat{x}_j(k)\|\right) \quad (17)$$
5. Update state and covariance matrix
   $$\hat{x}_i(k+1) = \hat{x}_i(k) + K * innov \quad (18)$$
   $$P_i(k+1) = P_i(k) - \frac{1}{S}P_i(k)dir_{ij}(k)dir_{ij}(k) \quad (19)$$

   end
6. Go to 1

2.4 | Simulation results

A Microsoft AirSim drone simulator [18] was used to evaluate the feasibility and performance of the proposed algorithms. This simulator provides realistic drone movements and sufficient application programming interfaces for effective FC. Because our objective is to reduce relative distance errors rather than guarantee accurate navigation, we used a simplified GNSS/INS method that acquires odometry values and 3D position measurements through a GNSS terminal, which assumes a true value, given zero-average Gaussian noise. We assume that each drone operates asynchronously, estimates the GNSS/INS data at 10 Hz, and has a random probability of successfully communicating with the other drones. When the drones communicate, they update their locations using the proposed algorithms.

Our experiment summoned four basic model drones to the vertices of a 10 × 10 m square in a neighborhood base map provided by AirSim (Figure 2A). Subsequently, the drones rotated and flew into an ellipse centered on different axes (Figure 2B), and the distance errors of each edge of the basic GNSS/INS and the one using the proposed algorithm were compared. Each episode was tested for 90 s over a total of 900 iterations. First, assuming that an average of 50 communication events occur in the total network each second, the relative distance error is measured when only the GNSS/INS is applied by the proposed algorithm. The results are shown in Figure 3, whose graphs reflect the distance errors of each edge. The blue graph indicates an error with the basic GNSS/INS, and the red graph indicates an error with the proposed GNSS/INS plus the proposed algorithm. At 80 s, the average error of the GNSS/INS was 1.43 m. However, when the proposed algorithm was applied, the average error was reduced to 0.56 m.

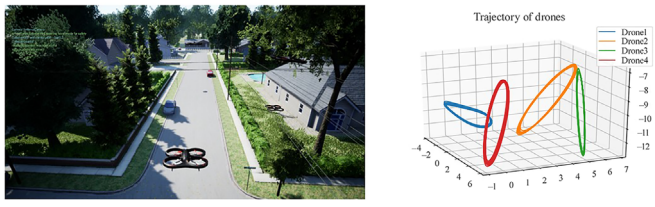

FIGURE 2 Simulation environment: (A) AirSim view, (B) drone motion in simulation.

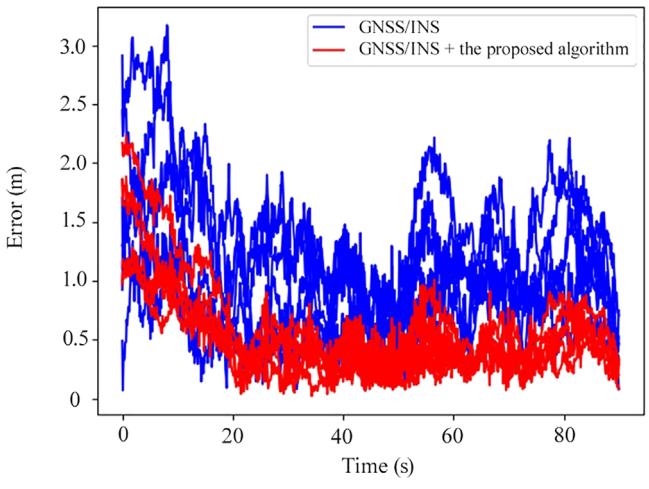

FIGURE 3 Graph comparing distance errors of all edges per iteration (blue graph: Global Navigation Support System (GNSS)/inertial navigation system (INS) only; red graph: GNSS/INS + proposed algorithm).

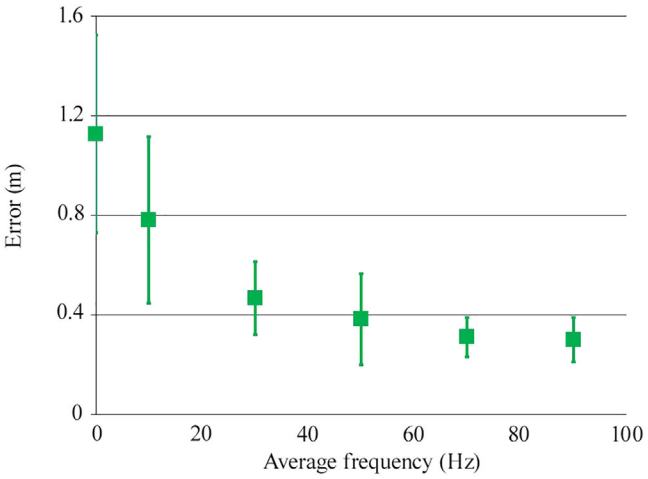

FIGURE 4 Graph of the proposed algorithm's distance errors per average communication frequency.

We also compared distance errors and average communication frequencies over multiple episodes. The sum of the relative distance errors at the last moment was measured (see Figure 4), and the average and standard deviation of the relative distance errors decreased with the average communication frequency. Thus, we can confirm that an optimal value can be derived by considering the desired performance and network load. Overall, the simulation results demonstrated good algorithmic feasibility and effectiveness.

3 | IMPLEMENTATION

3.1 | UWB asynchronous ranging and communication module

We developed a novel UWB ranging and communication module to implement our algorithm for real-world drone operations. This module serves as a data link capable of receiving commands from the FC and performing asynchronous transmissions and distance measurements. It includes a transmit mode and an always-on receive mode using a clear channel assessment (CCA) with a random-backoff protocol, which is suitable for random-access communications. It also implements the data exchange distance measurement function required for algorithmic operations.

The UWB communication module is based on Qorvo's DWM3000EVB, which combines a UWB antenna and a DW3000 communication chip. The module can be easily updated using firmware, and the communication and control levels can be adjusted through serial peripheral communication in one-frame units. The module is configured to use one channel (Channel 5), which

provides a maximum speed of 6.8 Mbps throughput. To implement the firmware, a NUCLEO-F429ZI board based on an STM32M4 core was selected, and a serial interface was configured for use with Pixhawk4 (see Figure 5).

Our proposed data-sharing distance measurement method reduces the number of frame transmissions and obtains data in real time by enabling data sharing between drones. The conventional UWB distance measurement method is single-side two-way ranging [19]; hence, Drone *i* performs distance measurements using two frames and sends the data using one frame. Drone *j* does the same, resulting in six frame exchanges. However, in a multidrone environment, increasing the number of frames leads to a higher probability of collisions. To mitigate this, a report frame that stores the calculated distance information (instead of time information) allows both drones to share the same distance information using the shared data (see Figure 6). The FC periodically stores the data to be shared in the module buffer and transmits them when a distance measurement attempt or request occurs. This enables the simultaneous exchange of distance and location data.

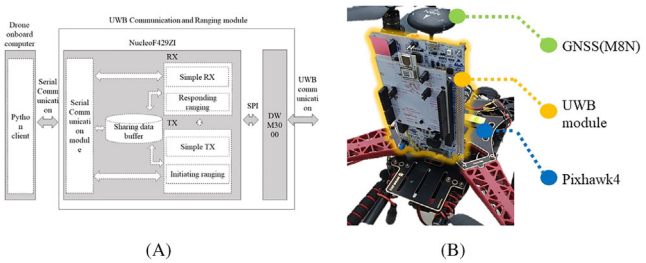

FIGURE 5 Configuration of asynchronous ultrawideband (UWB) ranging and communication module. (A) Hardware and software diagram of UWB communication module. (B) Appearance of UWB module installation.

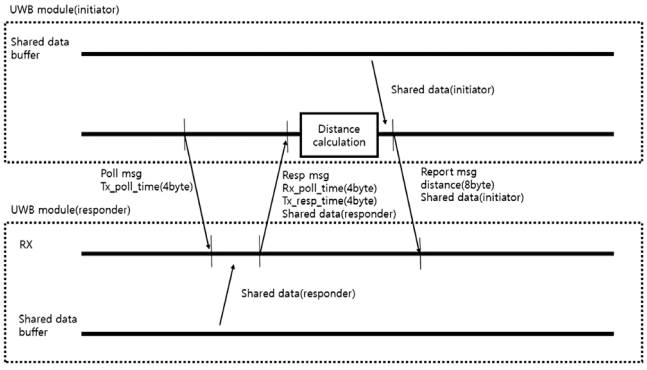

FIGURE 6 Distance measurement including data exchange diagram.

3.2 | Communication test

3.2.1 | Throughput, delay, and error rate tests

An experiment was conducted to measure the maximum speed and error rate of general data and distances to evaluate the performance of the new communication module. The experiment was conducted in an open playground with two modules placed 15 m apart. One module acted as a transmitter, and the others were receivers. The transmitter attempted to transmit general data or measure distances at maximum speed, whereas the receivers counted the number of frames arriving normally. The objective was to determine the performance limits of the communication module under ideal conditions. The experiments were divided into general data transmission/reception speed and error rate, data transmission/reception delay, and distance and error rate measurements.

In the second set of experiments, the performance of the communication module was measured in terms of general data transmission/reception delay. In the general experiment, the sending module recorded the sending time, and the receiving module recorded receipts and retransmission times. Communication delays were recorded by subtracting the sending time from the receipt time at the receiving module. A measured delay reflects the communication delay between FCs but not the delay between communication modules because the commands are given through the UWB module driver of the FC.

The maximum speed, error rate, and distance error of the distance measurement function were measured in the third experiment. The transmitting module transmitted distance measurement frames with 115 B of attached data at its maximum speed for 10 s. Subsequently, the receiving module recorded the number of successfully completed distance measurement frames. This experiment was repeated 10 times to obtain the distance measurement speed, distance measurement error, and measured distance error. The experimental results are listed in Table 2.

The average maximum transmission/reception speed of the data frame transmission was 428.0 Hz, and its standard deviation was 4.352 Hz. The error rate was 0.0%, the average delay was 4.329 ms, and the standard deviation was 0.3067 ms. The average range of the data-sharing speed was 242.0 Hz, and the standard deviation was 20 Hz. There was only one ranging error out of more than 20 000 frame exchanges; therefore, the error rate was considered to be 0%. The average distance error was 29 cm, and the standard deviation was 0.84 cm.

Based on the experimental results, the developed UWB communication module was found to be suitable for drone operations. The maximum rate of normal

TABLE 2 Communication performance of the UWB module.

	Data transmission			Ranging		
	Throughput (kbps)	Error rate (%)	Delay (ms)	Speed (Hz)	Error rate (%)	Distance error (cm)
Mean	393.7	0.0	4.329	242.0	0.0	29
Std.	3.937	0.0	0.306	20.00	0.0	0.84

Abbreviation: UWB, ultrawideband.

data-frame transmission and reception was 420 Hz, indicating no shortage in communication speed. This is significant because the maximum speed of the serial telemetry equipment installed in drones using Mavlink is 110 kbps, and this speed decreases when multimodule communication is supported. The maximum distance measurement transmission and reception speeds were high, and the distance measurement error was relatively low, indicating that the proposed distance measurement method is effective. However, the maximum length of the Mavlink frame is 250 B, which exceeds the 128 B currently supported by UWB communication devices. This indicates that further improvements are required to fully support drone communications.

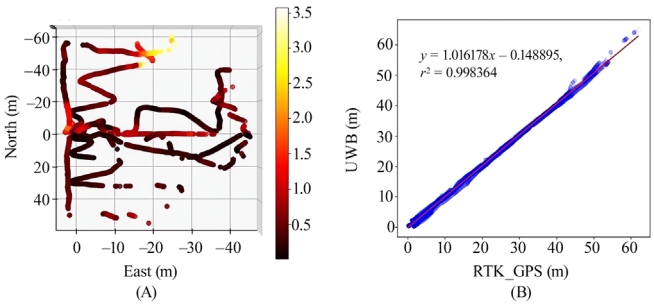

FIGURE 7 Ultrawideband (UWB) module range test. (A) Plot of distance error according to position. (B) Graph of UWB distance error versus real-time kinematic (RTK)-GPS based distance.

3.2.2 | Multiple access test

The speed and error rate of the developed communication module were measured experimentally in a multiaccess environment. Four communication modules were placed in a 10 × 10 m square on an open playground facing the center of the square. Each module attempted to transmit general data or measure the distance to another random module at intervals of 8–80 ms using a 115-B frame. This experiment lasted for 600 s, and the number of general data transmissions, receptions, and distance measurements were recorded to determine the average communication speed and error rate.

The results showed that all modules transmitted frames at an average rate of 9.752 Hz and measured distances at an average rate of 9.238 Hz. However, the error rates for general data communication and distance measurements were 8.25% and 13.06%, respectively. CCA was applied to avoid communication collisions, but significantly, high error rates were still obtained. This may have been caused by the other nodes attempting to communicate while exchanging ranging frames.

3.2.3 | Communication range test

The communication range of the UWB module was also measured, where two UWB communication modules and an RTK-GPS were prepared in an open field. RTK-GPS equipment can experimentally measure an object's true position at a 5-cm accuracy by correcting the GPS value. The two communication modules were set in advance to measure the true position in this fashion. The system was set to stop one module while attempting to measure the distance to another at 10 Hz; both modules' positions were recorded. One experimenter held the module and moved it around a hemispherical area centered on a stationary drone. The carried module was then directed toward the stationary drone, and the measured distances in each direction were compared.

The experimental results are shown in Figure 7. The maximum observed range was 44.36 m, and the average error was 54.85 cm with a maximum error of 3.58 m (see Figure 7A). Similar to prior research [20], the ranging performance exhibited variations based on the module's orientation. When the module was positioned backward, the error remained minimal, whereas it increased in the case of sparse communications. This behavior is likely attributable to antenna obstruction via the shape of the communication module. Figure 7B compares the distance values calculated using RTK-GPS and those obtained using UWB. A linear regression analysis was conducted, resulting in an approximation function of $y = 1.016178x - 0.148895, r^2 = 0.998364$. A graph plotting the UWB distance measurement values against the actual distances exhibited an error of approximately 1.5%.

3.3 | PX4 algorithm implementation

PX4 firmware was modified to implement the proposed algorithm and operate the UWB communication module. Customized firmware was developed by adding a UWB communication module driver and applying the proposed algorithm to an EKF2 measurement update in PX4 v1.13.1 [21]. The proposed algorithm was configured to operate at 10 Hz, with the probability of communicating with other drones set to 16% per iteration. The UWB distance measurement sensor noise, R, was set to 0.4 based on the average distance error obtained in a previous UWB distance measurement experiment.

UWB outlier rejection and landing situation response algorithms were added to ensure real-world functionality. Because UWB distance measurements are prone to excessive errors due to issues such as multipaths, an outlier rejection algorithm is essential. Although existing methods assume a certain level of difference from previous measurements for outlier rejection, they cannot be applied to our random communication-based approach. To overcome this limitation, we designed a new algorithm that identifies outlier data when the UWB measurement value exceeds a certain level based on the distance calculated using the exchanged GNSS/INS location estimate. In other words, the algorithm discards data if the absolute value of the innovation exceeds a threshold value, as shown in (20). The threshold was set to 5.0 m.

$$\left\| \left(z_{ij}(k) - \left\| \hat{x}_i(k) - \hat{x}_j(k) \right\| \right) \right\| < \text{threshold}. \tag{20}$$

In landing situations, the performance of the algorithm is enhanced through initializations. In the case of the PX4, the altitude was estimated during landing, which can lead to estimation errors before the flight. To mitigate this, we assumed that the drones were located on a flat plane and that the altitude error between them was zero during landing. We set $dir_{ij}(k)$'s z-position to zero and renormalized the vector when the drone landed.

4 | FIELD TEST

Field test is conducted to assess the feasibility and performance of the proposed algorithm in real-world scenarios. The experiments were designed to verify the algorithmic reduction in distance errors during formation flights. Four S500 frame drones equipped with the proposed UWB communication module, an algorithm-implemented Pixhawk4 FC, and an M8N GPS module were prepared. As shown in Figure 8A, the four drones

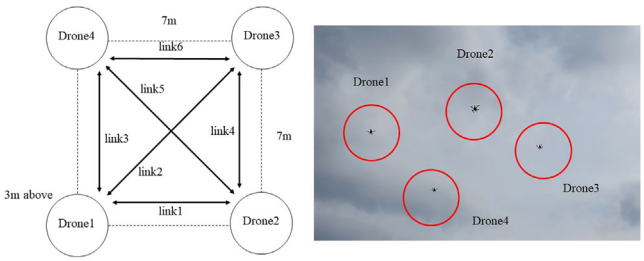

FIGURE 8 Field experiment of the proposed algorithm. (A) Configuration of formation flight. (B) Picture of formation flight in progress.

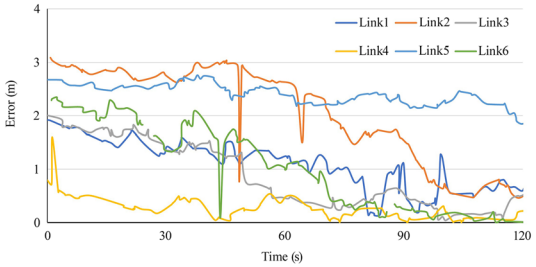

FIGURE 9 Distance error graphs according to time for each link.

were positioned at the vertices of a square 7 m per side, with the UWB communication module initially facing the center of the square. Each possible communication link among Drones 1–4 was assigned a number. During flight, the five drones maintained an upright triangular pyramid formation in which four drones were situated at each vertex of the base square with sides measuring 7 m. Drone 1 was elevated by 3 m to a position above the center of the bottom square to complete the shape.

A simple formation algorithm was applied to establish and maintain the formation. The operator was controlled only Drone 1, which broadcasts the control signals and its own flight information at a rate of 10 Hz via a UWB communication device. The surrounding drones used the acquired control signals and flight information to maintain their designated formation. The operator had the ability to command the activation and termination of an algorithm. Hence, when an algorithm was activated, all drones exchanged UWB distance measurements and data randomly with the other drones at an average rate of 1.6 Hz per link. The formation was set to hover at an altitude of 30 m, and the algorithm's performance was measured using UWB distance measurements and global position values. Data extracted from log files post-flight were analyzed. Furthermore, we analyzed the algorithmic efficiency based on the

microcontroller's recorded CPU and RAM metrics found in the PX4 log files.

The results confirm that the proposed algorithm effectively reduces the distance errors between drones. Figure 9 depicts the distance errors over time for each link. In the experiment, data were gathered while the drones hovered for 120 s. A distance error represents the difference between the UWB distance measurements and the calculated distances based on the global position values of each drone and its counterpart. Although the mean distance error was 2.12 m at $t = 0$, the error dropped to 0.63 m at 120 s, indicating a noticeable reduction over time. The graph occasionally exhibited spikes, which can be attributed to outliers as there were no significant changes in the positions of the drones. During the experiment, the CPU usage of the PX4 remained at 80%, and the RAM usage was 84%, confirming that the proposed algorithm can operate on the PX4 without significant strain.

5 | CONCLUSION

We proposed a loosely coupled UWB/GNSS/INS position-correction algorithm applicable to FCs that facilitates the control of airborne drone traffic via UWB random-access communications. The scheme was implemented by adding a measurement update to the existing EKF-based GNSS/INS navigation system, which is easy to apply. To demonstrate the feasibility of the proposed algorithm, an experiment was conducted using four flying drones in an AirSim simulator, showing that the algorithm reduces the average relative distance error by 31%. The standard deviation decreased by 16% when communicating at 10 Hz. We ran the algorithm for 120 s using a stationary formation flight of four drones equipped with UWB communication devices and the PX4 FC loaded with the new algorithm. From this experiment, we confirmed that the average distance error decreased from 2.12 m to 0.64 m, and we observed that, during the operation of the algorithm, CPU usage was 80% and RAM usage was 84%.

Our future plans involve calibrating UWB antennas to improve distance measurement precision [20]. We also aim to enhance the proposed algorithm to enable it to function in GNSS-denied environments. Through these endeavors, our objective is to expand the applicability of the single-drone optimal path-planning algorithm [22, 23] to encompass multidrone systems. This extension will facilitate further research on multidrone systems for indoor exploration.

ACKNOWLEDGMENTS

This study was supported by the Electronics and Telecommunications Research Institute (ETRI) grant funded by the Korean Government (23ZS1200, Fundamental Technology Research for Human-Centric Autonomous Intelligent Systems).

CONFLICT OF INTEREST STATEMENT

The authors declare that there are no conflicts of interest.

ORCID

Jeonggi Yang https://orcid.org/0000-0002-6746-2387

REFERENCES

1. H.G. Marina and E. Smeur, *Flexible collaborative transportation by a team of rotorcraft*, (Proc. International Conference on Robotics and Automation, Montreal, Canada), 2019, pp. 1074–1080.
2. A. Tagliabue, M. Kamel, S. Veriling, R. Siegwart, and J. Nieto, *Collaborative transportation using MAVs via passive force control*, (Proc. International Conference on Robotics and Automation, Singapore), 2017, pp. 5766–5773.
3. J. Gu, T. Su, Q. Wang, X. Du, and M. Guizani, *Multiple moving targets surveillance based on a cooperative network for multi-UAV*, IEEE Communic. Mag. **56** (2018), 82–89.
4. P. Schmuck and M. Chli, *Multi-UAV collaborative monocular SLAM*, (Proc. International Conference on Robotics and Automation, Singapore), 2017, pp. 3863–3870.
5. L. Bekmezci, O. K. Sahingoz, and S. Temel, *Flying ad hoc networks (FANETs): a survey*, Ad Hoc Netw. **3** (2013), 1254–1270.
6. F. Noor, M. A. Khan, A. Al-Zahrani, I. Ullah, and K. A. Al-Dhlan, *A review on communications perspective of flying AD-HOC networks: key enabling wireless technologies, applications, challenges and open research topics*, Drones **4** (2020), 65.
7. X. Lin, V. Yajnanarayana, S. D. Muruganathan, S. Gao, H. Asplund, H. L. Maattanen, M. Bergstrom, S. Euler, and Y. P. E. Wang, *The sky is not the limit: LTE for unmanned aerial vehicles*, IEEE Communic. Mag. **56** (2018), 204–210.
8. A. Guillen-Perez, R. Sanchez-Iborra, M. Cano, J.C. Sanchez-Aarnoutse, and J. Garcia-Haro, *WiFi networks on drones*, (Proc. ITU Kaleidoscope: ITU WT, Bangkok, Thailand), 2016, pp. 1–8.
9. P. R. Soria, A. F. Palomino, B.C. Arrue, and A. Ollero, *Bluetooth network for micro-UAVs for communication network and embedded range only localization*, (Proc. International Conference on Ummanned Aircraft System, Miami, FL, USA), 2017, pp. 747–752.
10. P. Sedlacek, M. Slanina, and P. Masek, *An overview of the IEEE 802.15. 4z standard its comparison and to the existing UWB standards*, (Proc. IEEE International Conference Radioelektronika Pardubice, Pardubice, Czech Republic), 2019, pp. 1–6.
11. K. Sivanand, *A UWB based localization system for indoor robot navigation*, (Proc. IEEE International Conference on Ultra-Wideband, Singapore), 2007, pp. 77–82.
12. S. Wang, *UWB-based localization for multi-UAV systems and collaborative heterogeneous multi-robot systems*, Procedia Comput. Sci. **175** (2020), 357–364.

13. T.M. Nguyen, A.H. Zaini, K. Guo, and L. Xie, *An ultra-wideband-based multi-UAV localization system in GPS-denied environments*, (Proc. International Micro Air Vehicles Conference, Beijing, China), 2016, pp. 1–15.
14. G. Kexin, X. Li, and L. Xie, *Ultra-wideband and odometry-based cooperative relative localization with application to multi-UAV formation control*, IEEE Trans. Cybernet. **50** (2019), 2590–2603.
15. H. Xu, L. Wang, Y. Zhang, K. Qiu, and S. Shen, Decentralized visual-inertial-UWB fusion for relative state estimation of aerial swarm, (Proc. IEEE ICRA_, Paris, France), 2020, pp. 8776–8782.
16. D. Pietra, V. P. Dabove, and M. Piras, *Loosely coupled GNSS and UWB with INS integration for indoor/outdoor pedestrian navigation*, Sensors **20** (2020), 6292.
17. W. Changqiang, *A seamless navigation system and applications for autonomous vehicles using a tightly coupled GNSS/UWB/INS/map integration scheme*, Remote Sens. (Basel) **14** (2021), no. 1, 27.
18. S. Shital D. Dey, C. Lovett, and A. Kapoor, *AirSim: high-fidelity visual and physical simulation for autonomous vehicles*, (Proc. Field and Service Robotics: Results of the 11th International Conference, Zurich, Switzerland), 2017, pp. 621–635.
19. IEEE Std. 802.15.4z-2020, IEEE standard for low-rate wireless networks–amendment 1: enhanced ultra-wideband (UWB) physical layers (PHYs) and associated ranging techniques, IEEE, 2020.
20. A. Ledergerber and R. D'andrea, *Calibrating away inaccuracies in ultra-wideband range measurements: a maximum likelihood approach*, IEEE Access **6** (2018), 78719–78730.
21. M. Lorenz, D. Honegger, and M. Pollefeys, *PX4: A node-based multithreaded open source robotics framework for deeply embedded platforms*, (Proc. IEEE ICRA, Seattle, WA, USA), 2015, pp. 6235–6240.
22. Y. Hong, S. Kim, Y. Kim, and J. Cha, *Quadrotor path planning using A* search algorithm and minimum snap trajectory generation*, ETRI J. **43** (2021), 1013–1023.
23. S. Jung, H. Lee, D. H. Shim, and A. al Agha-Mohammadi, *Collision-free local planner for unknown subterranean navigation*, ETRI J. **43** (2021), 580–593.

AUTHOR BIOGRAPHIES

Jeonggi Yang received his BS and MS degrees in Electrical Engineering from POSTECH, Pohang, South Korea, in 2016 and 2018, respectively. He is currently a researcher at the Electronics and Telecommunications Research Institute (ETRI). His research interests lie in control and its application to unmanned vehicle systems.

Soojeon Lee received his BS degree in Computer Science from Korea University in 2003 and the MS and PhD degrees in Computer Engineering from KAIST in 2005 and 2017, respectively. He is currently a principal researcher at ETRI. His research interests span the areas of computer networks, kernel architectures, high-performance computing systems, satellite ground systems, and drone simulation technology.

How to cite this article: J. Yang and S. Lee, *Ultrawideband coupled relative positioning algorithm applicable to flight controller for multidrone collaboration*, ETRI Journal **45** (2023), 758–767. DOI 10.4218/etrij.2023-0128